

## Evolution of collectivity with spin in $^{81}\text{Y}$

R. A. Kaye,<sup>1</sup> C. T. Rastovski,<sup>1,\*</sup> S. L. Tabor,<sup>2</sup> J. Döring,<sup>3,†</sup> F. Cristancho,<sup>4</sup> M. Devlin,<sup>5,‡</sup> G. D. Johns,<sup>6</sup> I. Y. Lee,<sup>7</sup> F. Lerma,<sup>5</sup>  
A. O. Macchiavelli,<sup>7</sup> D. G. Sarantites,<sup>5</sup> and G. Z. Solomon<sup>2</sup>

<sup>1</sup>*Department of Chemistry and Physics, Purdue University Calumet, Hammond, Indiana 46323*

<sup>2</sup>*Department of Physics, Florida State University, Tallahassee, Florida 32306*

<sup>3</sup>*Department of Physics, University of Notre Dame, Notre Dame, Indiana 46556*

<sup>4</sup>*Departamento de Física, Universidad Nacional de Colombia, Bogotá, Colombia*

<sup>5</sup>*Chemistry Department, Washington University, St. Louis, Missouri 63130*

<sup>6</sup>*Los Alamos National Laboratory, Los Alamos, New Mexico 87545*

<sup>7</sup>*Nuclear Science Division, Lawrence Berkeley National Laboratory, Berkeley, California 94720*

(Received 19 June 2002; published 13 November 2002)

Lifetimes of 34 high-spin levels in  $^{81}\text{Y}$  were measured using the Doppler-shift attenuation method. The high-spin states were populated using the  $^{58}\text{Ni}(^{32}\text{S},2\alpha p)$  reaction at 135 MeV, and the recoils were stopped in a thick Ta backing. Prompt multi- $\gamma$  coincidences were detected using GAMMASPHERE, and evaporated charged particles were detected with the MICROBALL. Transition quadrupole moments inferred from the lifetimes in the lowest positive- and negative-parity bands show a relatively gradual decrease with spin, in agreement with Hartree-Fock-Bogolyubov cranking calculations. The calculations also predict a shape change in each band from predominantly prolate at low spin to triaxial above the first quasiparticle alignment. Thus the observed decrease in collectivity with spin is interpreted as the result of competing shapes which tend to lower the amount of deformation. Other negative-parity bands show evidence for structures with large deformation.

DOI: 10.1103/PhysRevC.66.054305

PACS number(s): 21.10.Tg, 23.20.Lv, 27.50.+e

### I. INTRODUCTION

Previous studies of yttrium ( $Z=39$ ) isotopes have helped to illuminate several structural trends across the  $f-p-g$  shell. One of the most important underlying causes of these trends concerns the quasiparticle occupation of the available single-particle energy levels near the proton and neutron Fermi surfaces. For example, near the  $N=50$  shell closure, angular momentum and energy are built primarily through successive single-particle alignments rather than through collective excitations, as observed in  $^{85}\text{Y}$  [1] and  $^{87-90}\text{Y}$  [2–5]. Closer to midshell ( $N=39$ ), the degree of collectivity is enhanced strongly relative to the single-particle estimate, demonstrated by studies of  $^{82}\text{Y}$  [6,7] and  $^{83}\text{Y}$  [8]. Large deformations are thus anticipated for particle numbers near the mid-shell value.

Another interesting aspect of shell occupation is its effect on structure with increasing spin. In particular, the prolate deformed shell gap at particle number 38 ( $\beta_2=0.4$ ) plays an important role in deciding the high-spin structure of nuclei with  $N$  and/or  $Z$  numbers near this gap. Studies of the light Y isotopes have provided valuable information about the influence of single-particle level occupation just above this gap. While  $^{82}\text{Y}$  shows relatively constant  $B(E2)$  values at high spin [6,7], a high-spin study of  $^{83}\text{Y}$  [8] indicated that the  $Q_t$  moments in the positive-parity yrast band generally decreased with spin, yet this sequence did not seem to be losing

collectivity into a single-particle band termination [9] as the maximum spin in the  $f-p-g$  shell was reached. Below the gap, the proton-rich krypton ( $Z=36$ ), rubidium ( $Z=37$ ), and strontium ( $Z=38$ ) isotopes, which already have relatively large equilibrium deformations, have shown evidence of rigid rotation at high spin based on nearly constant transition quadrupole moments  $Q_t$  in the range of about  $2-4\text{eb}$  in the yrast bands [10–16]. Furthermore, drops in the  $Q_t$  moments in  $^{79}\text{Sr}$  were associated [17] with the onset of quasiparticle alignment. More investigations appear necessary to determine how these traits develop for nuclei closer to the  $N\approx Z$  line.

A previous investigation [18] measured the lifetimes of five states in the yrast positive-parity band of the  $N=Z+3$  nucleus  $^{81}\text{Y}$  using the Doppler-shift attenuation method and the recoil-distance method. The results were based on a level scheme constructed from their work and prior investigations [19–21]. Since then, a more comprehensive level scheme was developed with multiple positive- and negative-parity band structures extending to considerably high-spin values of  $I\approx\frac{55}{2}$  [22]. Figure 1 shows a partial level scheme of  $^{81}\text{Y}$  based on these results. By extending the yrast positive- and negative-parity bands to high spin, evidence of possible band termination was discovered. In addition, one of the negative-parity bands was thought to be a possible candidate for superdeformation based on its fragmentary decay near the band head and the high and constant moments of inertia, characteristic of other superdeformed bands in this mass region ( $^{83}\text{Sr}$  [23], for example). So far, however, the collectivity of  $^{81}\text{Y}$  has not been determined for any negative-parity band, and the collectivity of the yrast positive-parity band has not been established at high spin above the first quasiparticle alignment [22].

The present work investigated the evolution of collectivity

\*Present address: Department of Physics, University of Illinois at Chicago, Chicago, Illinois 60612.

†Present address: GSI, 64291 Darmstadt, Germany.

‡Present address: Los Alamos National Laboratory, Los Alamos, New Mexico 87545.

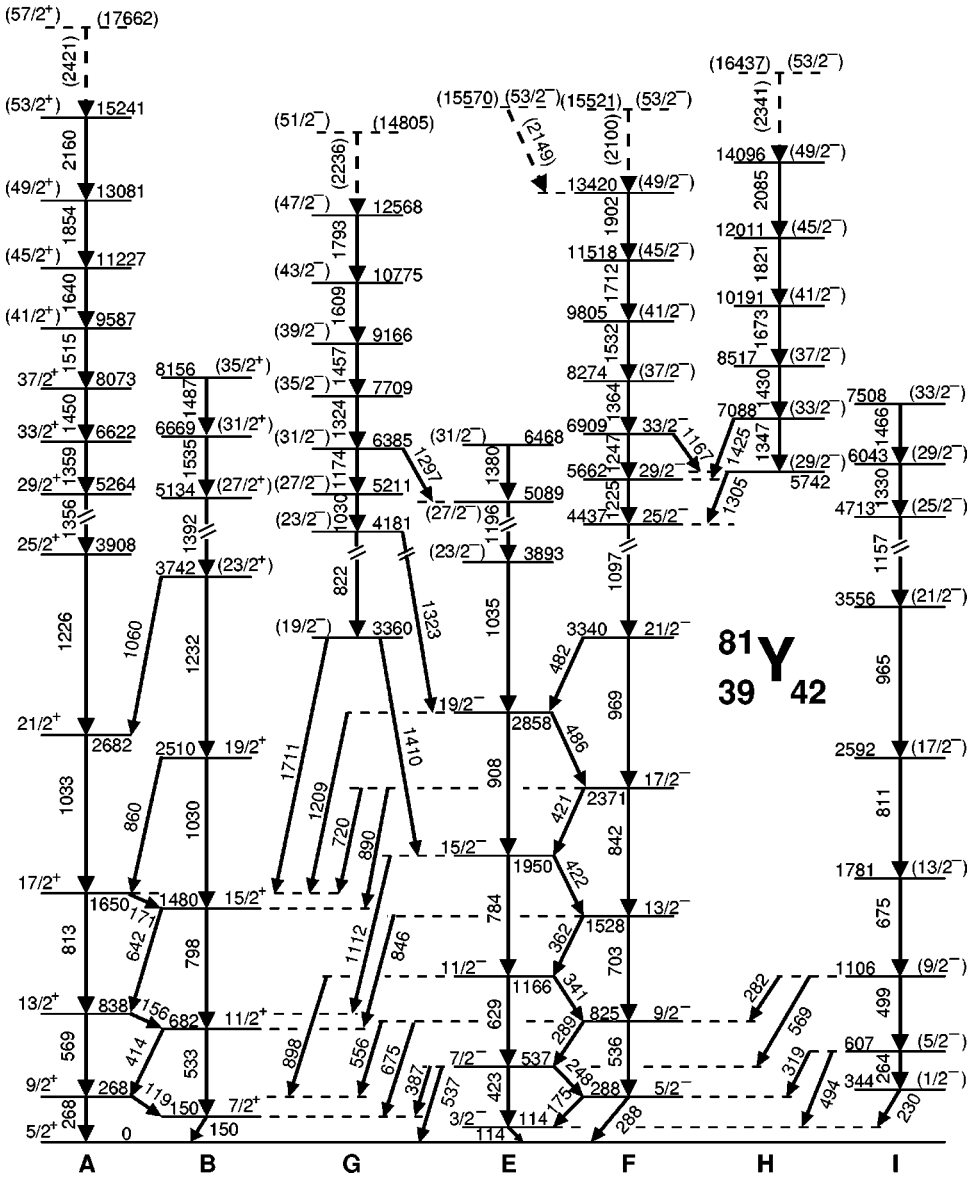


FIG. 1. Partial level scheme of  $^{81}\text{Y}$  [22] showing the bands in which lifetimes were measured in the present work. The vertical energy scale is reduced by a factor of four above an excitation energy of 4000 keV. The letters below the decay sequences are intended only to facilitate the discussion and follow the same convention as in Ref. [22].

ity with spin in  $^{81}\text{Y}$  for as many positive- and negative-parity band structures as possible, in order to provide a more complete picture of the degree of collectivity for this nucleus and for nuclei near the  $N, Z = 38$  gap. The Doppler-shift attenuation method was used to measure lifetimes less than about 1 ps, from which transition strengths were calculated and used to infer transition quadrupole moments using the rotational model. The measurement utilized the GAMMASPHERE  $\gamma$ -detector array [24] and the MICROBALL  $4\pi$  charged-particle array [25] to help accentuate the  $\gamma$ -decay events from this weak reaction channel.

As a result of this work, the collectivity of an  $N \approx Z$  nucleus has been at least partially established at relatively high spin for both positive- and negative-parity structures, providing information on the mechanisms responsible for the measured variations with rotational frequency. In addition, the observed evolution of collectivity with spin has demonstrated the importance of the interplay of single-particle and collective degrees of freedom.

## II. EXPERIMENTAL PROCEDURE

High-spin states in  $^{81}\text{Y}$  were produced following the  $^{58}\text{Ni}(^{32}\text{S}, 2ap)$  fusion-evaporation reaction at 135 MeV using the 88-in. Cyclotron facility at the Lawrence Berkeley National Laboratory. In order to optimize the experiment for the detection of Doppler-shifted  $\gamma$ -ray line shapes and hence the measurement of lifetimes using the Doppler-shift attenuation method, the  $415 \mu\text{g}/\text{cm}^2$  thick  $^{58}\text{Ni}$  target was evaporated on to a  $10.3 \text{ mg}/\text{cm}^2$  Ta backing which served to stop completely all recoiling nuclei. The average initial recoil velocity of  $^{81}\text{Y}$  nuclei was  $\beta = 0.034$ . The reaction was designed to synthesize mass 86 nuclei, so  $^{81}\text{Y}$  was only weakly produced at about 3% of the total fusion cross section. However, the methods of particle and gamma detection allowed for a detailed lifetime measurement of this nucleus nonetheless.

Prompt  $\gamma$  rays were detected using the GAMMASPHERE array [24] with 95 Compton-suppressed Ge detectors.

Evaporated charged particles were detected and identified with the MICROBALL array [25], consisting of 95 CsI(Tl) scintillators covering 97% of the full sphere surrounding the target. During the experiment, a four-fold or higher  $\gamma$  multiplicity trigger condition was used.

The collected data were sorted in a variety of ways into  $3000 \times 3000$  channel square  $\gamma$ - $\gamma$  coincidence matrices with a dispersion of 1.333 keV/channel. In order to enhance the  $^{81}\text{Y}$  reaction channel, all matrices were gated on the requirement of a  $2\alpha + p$  evaporation event as measured by the MICROBALL. Most of the matrices had any remaining contaminations (such as the relatively strong  $^{83}\text{Y}$  channel) further reduced by gating them on the requirement of an additional coincident  $\gamma$  ray. Positive-parity transitions were enhanced by selecting the 119, 150, 156, 268, 414, 533, 569, 642, 798, 813, or 860 keV line as the possible coincident  $\gamma$  ray. Negative-parity transitions were enhanced by selecting the 114, 175, 248, 288 (doublet), 341, 362, 422 (doublet), 499, 556, 629, 675, 703, or 784 keV line as the gating transition.

Gamma-ray intensities were measured in order to quantify the amount of direct and side feeding. Branching ratios, needed for the determination of transition strengths and quadrupole moments, were deduced from these intensities. The results are generally in good agreement with those measured previously [18] whenever comparisons were possible. Lineshape spectra were obtained by projecting on square matrices built from coincidences between sets of detectors with approximately the same  $\theta$  angle and all other detectors. By combining detector rings at  $31.72^\circ$  with  $37.38^\circ$ ,  $50.07^\circ$  with  $58.28^\circ$ ,  $121.72^\circ$  with  $129.93^\circ$ , and  $142.62^\circ$  with  $148.28^\circ$ , weighted average detector angles of  $34.95^\circ$  (7 active detectors),  $52.81^\circ$  (15 active detectors),  $127.19^\circ$  (15 active detectors), and  $145.45^\circ$  (10 active detectors) were obtained and used for lineshape analysis. This process improved the statistics of each line shape and has been shown [26] to yield nearly identical results as the process of summing the separate spectra of detectors at each similar ring angle.

### III. ANALYSIS METHOD

Mean lifetimes of excited states in the bands shown in Fig. 1 were measured by applying the Doppler-shift attenuation method (DSAM) to the experimental line shapes at  $34.95^\circ$ ,  $52.81^\circ$ ,  $127.19^\circ$ , and  $145.45^\circ$ . The DSAM involves a comparison of the decay time of the recoiling nuclei with their slowing-down time in the target and target backing foil. This comparison was carried out using the simulation code FITS [27] which integrates over the thickness of the target and determines a Gaussian distribution of recoil velocities (with a width that is 10% of the kinematic mean) at the time of decay, thus accounting for the evaporation of charged particles in the reaction. It corrects for direct feeding from up to four known higher-lying states and side feeding from one unknown state, as well as for finite detector solid angle and resolution and the energy dependence of the reaction cross sections as the beam slows through the target. The nuclear and electronic stopping powers were obtained from program SRIM2000, a recent compilation of the work of Refs. [28,29].

By varying the lifetime of the state of interest, a set of

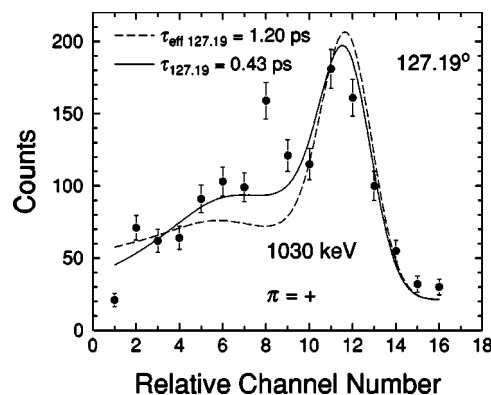


FIG. 2. Fits to the  $127.19^\circ$  line shape of the 1030 keV transition in band B with (corrected, solid line) and without (effective, dashed line) feeding corrections.

theoretical line shapes were produced and compared with the measured Doppler-shifted spectrum at each average detector angle to find the best fit. The lifetime which generated a curve that had the lowest reduced  $\chi^2$  when compared to the experimental spectrum was taken as the lifetime of that state. The uncertainty of individual lifetimes at each average detector angle was determined by finding the lifetime value above and below the best fit value which increased the minimum reduced  $\chi^2$  value by one unit. The accepted lifetime values were determined from an average of the individual lifetimes. The uncertainties in the accepted lifetimes were deduced from either the standard deviation of the set of individual lifetimes or the uncertainties in the individual lifetime fits, whichever was larger.

Effective lifetimes, which do not include feeding corrections, were first determined for each line shape with adequate statistics. All line shapes were then refit with feeding corrections, with the exception of those from the highest fitted transition in each band, where only an upper-limit effective lifetime could be obtained. The feeding corrections used the effective lifetime of the state (or possibly multiple states) immediately above and, where necessary, one side-feeding state to feed the state of interest. A comparison of fits to a 1030 keV (band B transition) line shape with (corrected) and without (effective) feeding corrections is shown in Fig. 2.

Whenever possible, mean lifetimes were determined from spectra gated from above (GFA) the transitions of interest, eliminating the effects of side feeding. In these cases, the transitions were also gated from below (GFB) for the determination of side-feeding times and as a test of consistency. The total side-feeding intensities were obtained from the intensity balance of each state, and the side-feeding lifetime was allowed to vary until the mean lifetime agreed with the GFA result. Figure 3 displays a GFA and GFB fit to the 1226 keV transition in band A.

Limited statistics often forced the use of only a GFB fit to an experimental line shape. In these situations, the side-feeding times used in the feeding corrections were based on the results obtained from fitting side-feeding times in both the yrast positive- and negative-parity bands. Averaging the results showed that the side-feeding times were about 94% of the effective lifetime of the state above, and this average was

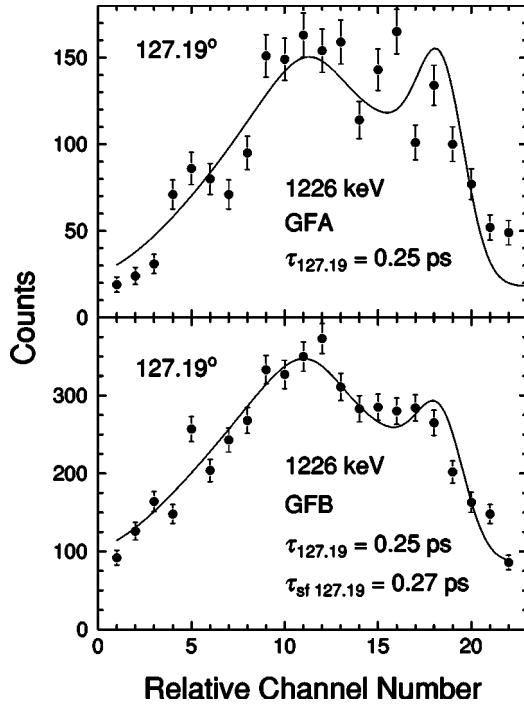


FIG. 3. Fits to the  $127.19^\circ$  line shape of the 1226 keV transition in band A gated from above (GFA) and gated from below (GFB). A side-feeding time of 0.27 ps was measured for the  $\frac{25}{2}^+$  state from this fit.

adopted for all GFB fits. A similar result was obtained for  $^{83}\text{Y}$  [30], where the measured side-feeding times in the yrast positive-parity band averaged about 83% of the effective lifetime of the state above. Regardless of this agreement, the resulting mean lifetimes in the present work were rather insensitive to the side-feeding time as long as the side-feeding intensity was small.

The line shape analysis was complicated by the fact that  $^{81}\text{Y}$  has several closely spaced doublets in the decay scheme, many of which are in coincidence with each other (see Fig. 1). In most cases, it was possible to fit each transition without interference from other peaks by using a careful choice of gates. Sometimes this required the use of matrices not gated on an additional coincident  $\gamma$  ray in order to increase the statistics when only one or two gates were used to obtain the line shape. When high lying, strongly shifted peaks were used as gates, the gate was set wide enough to include all possible shifted energies, although this procedure worked best for matrices already gated by an additional coincident  $\gamma$  ray in order to reduce the inclusion of contaminant peaks from other nuclei.

When it was not possible to resolve individual line shapes, a modified version of FITS was used to fit two overlapping line shapes simultaneously with theoretical line shapes properly scaled by the intensity of each  $\gamma$  ray. Figure 4 shows an example of a simultaneous fit to the 1030 keV transition in band G and the 1035 keV transition in band E. A similar procedure was used to fit the 1356 and 1359 keV lines in band A. The results were fairly consistent for all four average detector angles, as shown in Table I.

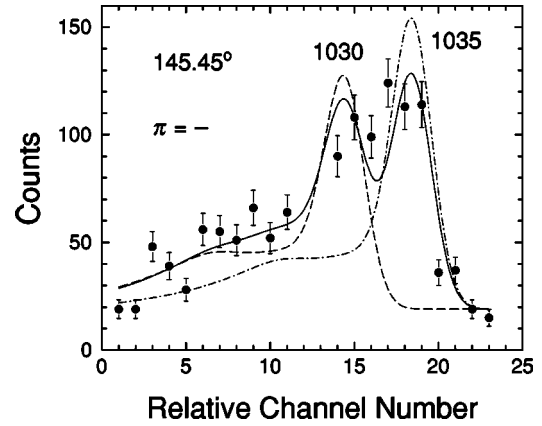


FIG. 4. Simultaneous fit to the line shapes of the 1030 keV transition in band G and the 1035 keV transition in band E measured at  $145.45^\circ$ . The broken curves show the individual contributions of each line shape to the overall best fit (solid line) before scaling by the relative intensity of each  $\gamma$  ray.

#### IV. RESULTS

Lifetimes of 34 states were measured using the DSAM and are given in Table I. The effective lifetimes represent the average of the results obtained from each of the average detector angles for which they could be measured. Mean lifetimes, which include feeding corrections, are given for each average detector angle along with the accepted lifetime which represents the average of these results. If a reliable line shape could not be obtained at a particular angle, a lifetime result is not included in the table. Results from a previous lifetime analysis of  $^{81}\text{Y}$  [18] are also included in Table I for comparison ( $\tau_{\text{prev}}$ ). Fits to the 1425-keV transition between bands F and H at all four average detector angles are shown in Fig. 5 to demonstrate the variation of the line shape with angle.

##### A. Positive-parity states

Lifetimes were measured in the yrast positive-parity bands (bands A and B in Fig. 1) up to the  $(\frac{49}{2}^+)$  state in band A and the  $(\frac{27}{2}^+)$  state in band B by summing as many clean GFB spectra as possible. Line shapes could not be extracted above these levels, so only effective lifetimes are quoted for these states.

The line shapes of the 1356, 1359, 1450, 1515, and 1640 keV transitions in band A were all obtained from summing GFB spectra projected from a triple-coincidence matrix. A simultaneous fit was performed to the 1356 and 1359 keV lines in order to decompose their line shapes and extract lifetimes individually for the 5264 keV  $\frac{29}{2}^+$  and 6622 keV  $\frac{33}{2}^+$  states, respectively. It was possible to extract reliable GFA spectra for the 813, 1033, and 1226 keV  $\gamma$  rays in this band, and hence the quoted mean lifetimes associated with the states they decay result from a GFA analysis. The results are in excellent agreement with the lifetimes measured previously for these states [18] (see Table I).

An interesting feature of band A is the nearly constant effective lifetimes of the  $\frac{37}{2}^+$ ,  $(\frac{41}{2}^+)$ , and  $(\frac{45}{2}^+)$  states. Such

TABLE I. Effective and mean lifetimes measured for  $^{81}\text{Y}$ . The effective lifetimes ( $\tau_{\text{eff}}$ ) and accepted mean lifetimes ( $\tau_{\text{acc}}$ ) represent the average of results at all possible average detector angles. Excitation energies ( $E_x$ ),  $\gamma$ -ray energies ( $E_\gamma$ ), and spins were taken from Ref. [22].

$E_x$ (keV)	$I_i^\pi$ ( $\hbar$ )	$I_f^\pi$ ( $\hbar$ )	$E_\gamma$ (keV)	$\tau_{\text{prev}}^a$ (ps)	$\tau_{\text{eff}}$ (ps)	$\tau$ (ps)	34.95°	52.81°	127.19°	145.45°	$\tau_{\text{acc}}$ (ps)
Band A											
13081	$(\frac{49}{2}^+)$	$(\frac{45}{2}^+)$	1854		$0.18_{-12}^{+32}$						
11227	$(\frac{45}{2}^+)$	$(\frac{41}{2}^+)$	1640		$0.32_{-16}^{+30}$	$0.08_{-7}^{+20}$	$0.14_{-13}^{+19}$	$0.02_{-1}^{+9}$	$0.04_{-3}^{+9}$	$0.07_{-6}^{+14}$	
9587	$(\frac{41}{2}^+)$	$(\frac{37}{2}^+)$	1515		$0.30_{-12}^{+16}$	$0.02_{-1}^{+8}$	$0.04_{-3}^{+5}$	$0.03_{-2}^{+8}$	$0.06_{-5}^{+13}$	$0.04_{-3}^{+8}$	
8073	$(\frac{37}{2}^+)$	$(\frac{33}{2}^+)$	1450		$0.35_{-8}^{+9}$	$0.16_{-7}^{+7}$	$0.18_{-8}^{+10}$	$0.04_{-3}^{+4}$	$0.06_{-5}^{+6}$	$0.11_{-6}^{+7}$	
6622	$(\frac{33}{2}^+)$	$(\frac{29}{2}^+)$	1359		$0.44_{-8}^{+8}$	$0.11_{-3}^{+3}$	$0.15_{-4}^{+4}$	$0.10_{-2}^{+2}$	$0.14_{-4}^{+4}$	$0.12_{-3}^{+3}$	
5264	$(\frac{29}{2}^+)$	$(\frac{25}{2}^+)$	1356	$<0.29^b$	$0.40_{-10}^{+10}$	$0.05_{-1}^{+2}$	$0.06_{-2}^{+2}$	$0.11_{-3}^{+3}$	$0.13_{-3}^{+4}$	$0.09_{-4}^{+4}$	
3908	$(\frac{25}{2}^+)$	$(\frac{21}{2}^+)$	1226	$0.22_{-9}^{+9}$	$0.58_{-6}^{+8}$	$0.20_{-5}^{+7c}$	$0.14_{-4}^{+4c}$	$0.25_{-6}^{+7c}$	$0.28_{-5}^{+6c}$	$0.22_{-6}^{+6c}$	
2682	$(\frac{21}{2}^+)$	$(\frac{17}{2}^+)$	1033	$0.49_{-10}^{+14}$	$1.37_{-25}^{+25}$	$0.39_{-7}^{+8c}$	$0.32_{-6}^{+7c}$	$0.36_{-6}^{+7c}$	$0.41_{-7}^{+8c}$	$0.37_{-6}^{+7c}$	
1650	$(\frac{17}{2}^+)$	$(\frac{13}{2}^+)$	813	$0.95_{-20}^{+30}$	$3.90_{-87}^{+154}$	$0.96_{-32}^{+71c}$	$1.00_{-26}^{+43c}$	$1.00_{-26}^{+44c}$	$0.96_{-17}^{+26c}$	$0.98_{-25}^{+46c}$	
838	$(\frac{13}{2}^+)$	$(\frac{9}{2}^+)$	569	$4.3_{-6}^{+6}$						$4.3_{-6}^{+6}$	
Band B											
5134	$(\frac{27}{2}^+)$	$(\frac{23}{2}^+)$	1392		$0.36_{-12}^{+14}$						
3742	$(\frac{23}{2}^+)$	$(\frac{19}{2}^+)$	1232		$0.57_{-17}^{+13}$	$0.26_{-14}^{+17}$	$0.27_{-12}^{+14}$	$0.17_{-8}^{+9}$	$0.21_{-8}^{+11}$	$0.23_{-10}^{+13}$	
2510	$(\frac{19}{2}^+)$	$(\frac{15}{2}^+)$	1030		$1.10_{-20}^{+34}$	$0.44_{-15}^{+26}$	$0.31_{-9}^{+12}$	$0.43_{-10}^{+13}$	$0.43_{-12}^{+17}$	$0.40_{-12}^{+17}$	
1480	$(\frac{15}{2}^+)$	$(\frac{11}{2}^+)$	798		$\approx 4$	$>1$	$>1$	$>1$	$>1$	$>1$	
Band E											
6468	$(\frac{31}{2}^-)$	$(\frac{27}{2}^-)$	1380		$0.50_{-17}^{+24}$						
5089	$(\frac{27}{2}^-)$	$(\frac{23}{2}^-)$	1196		$0.58_{-16}^{+22}$	$0.10_{-9}^{+15}$	$0.22_{-13}^{+16}$	$0.10_{-9}^{+10}$	$0.18_{-14}^{+19}$	$0.15_{-11}^{+15}$	
3893	$(\frac{23}{2}^-)$	$(\frac{19}{2}^-)$	1035		$1.62_{-29}^{+48}$	$0.53_{-15}^{+26}$	$0.64_{-14}^{+21}$	$0.58_{-11}^{+14}$	$0.79_{-24}^{+25}$	$0.64_{-16}^{+21}$	
2858	$(\frac{19}{2}^-)$	$(\frac{15}{2}^-)$	908		$2.94_{-82}^{+223}$			$0.80_{-31}^{+72}$	$0.49_{-21}^{+48}$	$0.64_{-26}^{+60}$	
Band F											
11518	$(\frac{45}{2}^-)$	$(\frac{41}{2}^-)$	1712		$0.16_{-8}^{+14}$						
9805	$(\frac{41}{2}^-)$	$(\frac{37}{2}^-)$	1532		$0.24_{-11}^{+20}$	$0.06_{-5}^{+10}$	$0.02_{-1}^{+10}$	$0.02_{-1}^{+5}$	$0.03_{-2}^{+7}$	$0.03_{-2}^{+8}$	
8274	$(\frac{37}{2}^-)$	$(\frac{33}{2}^-)$	1364		$0.35_{-13}^{+23}$	$0.03_{-2}^{+6}$	$0.45_{-19}^{+23}$	$0.04_{-3}^{+7}$	$0.04_{-3}^{+13}$	$0.14_{-11}^{+21}$	
6909	$(\frac{33}{2}^-)$	$(\frac{29}{2}^-)$	1247		$0.40_{-15}^{+23}$	$0.30_{-29}^{+59}$	$0.12_{-11}^{+12}$	$0.19_{-10}^{+11}$		$0.20_{-16}^{+20}$	
5662	$(\frac{29}{2}^-)$	$(\frac{25}{2}^-)$	1225		$0.55_{-11}^{+14}$	$0.18_{-7}^{+9}$	$0.15_{-7}^{+8}$	$0.14_{-6}^{+8}$	$0.22_{-8}^{+8}$	$0.17_{-7}^{+8}$	
4437	$(\frac{25}{2}^-)$	$(\frac{21}{2}^-)$	1097		$0.82_{-12}^{+15}$	$0.29_{-16}^{+28c}$	$0.27_{-9}^{+14c}$	$0.23_{-8}^{+11c}$	$0.19_{-11}^{+16c}$	$0.24_{-11}^{+17c}$	
3340	$(\frac{21}{2}^-)$	$(\frac{17}{2}^-)$	969		$1.50_{-23}^{+34}$	$0.40_{-14}^{+26c}$	$0.38_{-12}^{+15c}$	$0.35_{-9}^{+12c}$	$0.40_{-10}^{+16c}$	$0.38_{-11}^{+17c}$	
2371	$(\frac{17}{2}^-)$	$(\frac{13}{2}^-)$	842		$4.14_{-120}^{+338}$	$0.94_{-38}^{+103c}$	$0.76_{-27}^{+60c}$	$0.62_{-19}^{+30c}$	$0.76_{-26}^{+54c}$	$0.77_{-28}^{+62c}$	
Band G											
6385	$(\frac{31}{2}^-)$	$(\frac{27}{2}^-)$	1174		$0.53_{-20}^{+32}$						
		$(\frac{27}{2}^-)$	1297		$0.53_{-20}^{+32}$						
5211	$(\frac{27}{2}^-)$	$(\frac{23}{2}^-)$	1030		$1.27_{-47}^{+47}$	$0.43_{-13}^{+17}$	$0.22_{-4}^{+4}$	$0.44_{-9}^{+13}$	$0.63_{-16}^{+30}$	$0.43_{-17}^{+17}$	
4181	$(\frac{23}{2}^-)$	$(\frac{19}{2}^-)$	822		$2.76_{-120}^{+120}$	$1.10_{-80}^{+900}$	$0.92_{-64}^{+900}$	$1.00_{-71}^{+900}$	$0.82_{-70}^{+900}$	$0.96_{-71}^{+900}$	
Band H											
8517	$(\frac{37}{2}^-)$	$(\frac{33}{2}^-)$	1430		$0.32_{-10}^{+10}$						
7088	$(\frac{33}{2}^-)$	$(\frac{29}{2}^-)$	1425		$0.39_{-10}^{+12}$	$0.08_{-7}^{+14}$	$0.06_{-4}^{+6}$	$0.05_{-4}^{+5}$	$0.10_{-5}^{+7}$	$0.07_{-5}^{+8}$	
5742	$(\frac{29}{2}^-)$	$(\frac{25}{2}^-)$	1305		$0.46_{-14}^{+20}$	$0.17_{-16}^{+17}$	$0.10_{-9}^{+12}$	$0.29_{-12}^{+14}$	$0.48_{-14}^{+21}$	$0.26_{-15}^{+17}$	
Band I											
4713	$(\frac{25}{2}^-)$	$(\frac{21}{2}^-)$	1157		$1.18_{-32}^{+95}$						
3556	$(\frac{21}{2}^-)$	$(\frac{17}{2}^-)$	965		$1.51_{-34}^{+70}$		$0.24_{-17}^{+30}$	$0.36_{-20}^{+35}$	$0.27_{-15}^{+27}$	$0.29_{-17}^{+30}$	
2592	$(\frac{17}{2}^-)$	$(\frac{13}{2}^-)$	811			$>1$	$0.76_{-33}^{+94}$	$>1$	$>1$	$>1$	

<sup>a</sup>From Ref. [18].

<sup>b</sup>Effective lifetime.

<sup>c</sup>Determined from spectra gated from above (GFA) the transition.

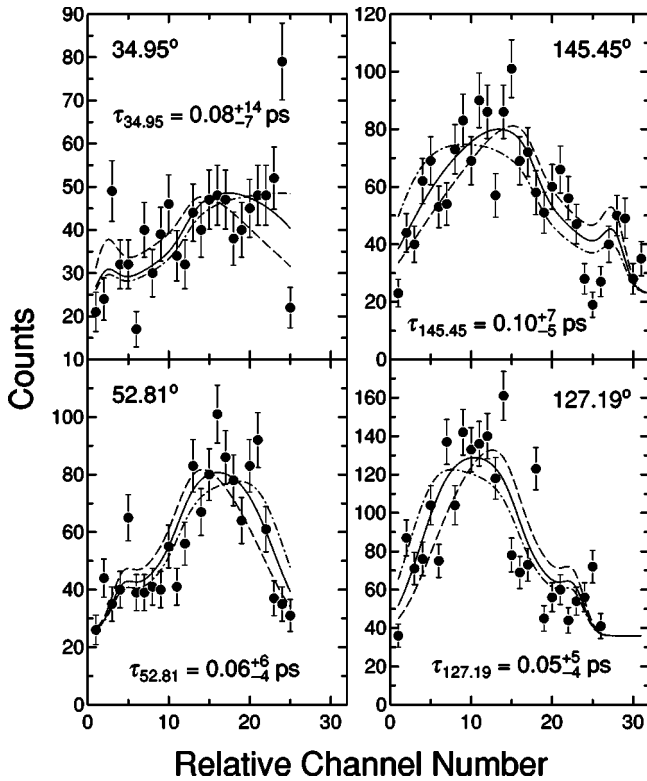


FIG. 5. Fits to the line shapes of the 1425 keV decay of band H at all four average detector angles. The uncertainty limits of the best fit (solid curve) are indicated by the dashed and dash-dotted curves.

behavior is not typical of rotational bands, where the effective lifetimes usually decrease steadily with excitation energy. The effect of the relatively constant effective lifetimes of these three states in band A caused a large feeding correction to the  $(\frac{41}{2}^+)$  state, and hence resulted in a relatively short mean lifetime for this state compared to the  $\frac{37}{2}^+$  and  $(\frac{45}{2}^+)$  states. Figure 6 shows the  $52.81^\circ$  line shapes of the 1450, 1515, and 1640 keV transitions in band A. The rather large uncertainty in the lifetime of the  $(\frac{41}{2}^+)$  state reflects the impact of the large feeding correction.

The line shapes of the 1030 and 1232 keV lines in band B were generated from spectra GFB these transitions. In order to avoid contamination by the much stronger 1033 and 1226 keV transitions in band A, only gates on the 642, 798, and 860 keV lines were used to obtain the line shapes. (The 642 and 798 keV lines show only a very weak coincidence with the 1033 keV line through the very low intensity 171 keV linking transition between bands A and B.) These gates were mostly clean of lines from other nuclei, so the gate projections were made on the double-coincidence matrix to improve the lineshape statistics. A GFA line shape was obtained for the 798 keV transition, but during the fitting process the corrected lifetime did not converge above 1 ps. Since the DSAM technique tends not to be as reliable above 1 ps, only a lower limit lifetime is given for the  $\frac{15}{2}^+$  state.

### B. Negative-parity states

Lifetimes were measured in the yrast negative-parity states (bands E and F in Fig. 1) up to the  $(\frac{31}{2}^-)$  state in band

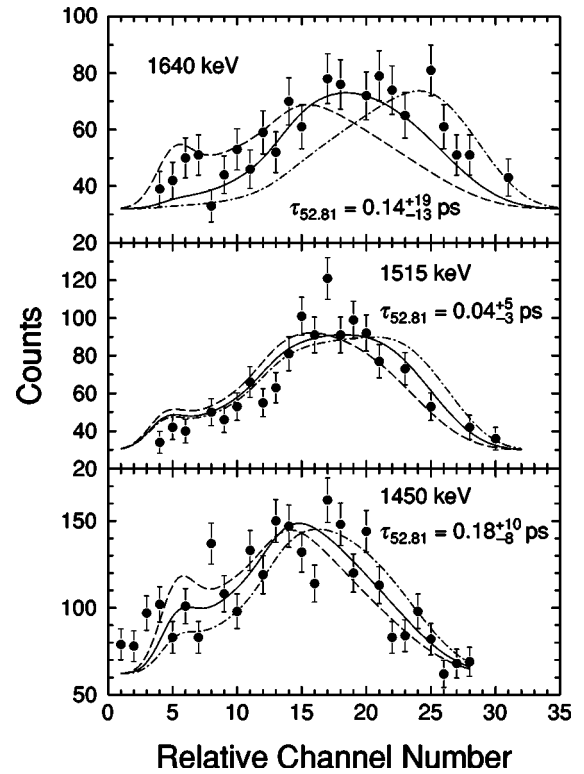


FIG. 6. Fits to the  $52.81^\circ$  line shapes of the 1450, 1515, and 1640 keV transitions in band A. The uncertainty limits of the best fit (solid curve) are indicated by the dashed and dash-dotted curves.

E and the  $(\frac{45}{2}^-)$  state in band F. In addition, lifetimes were measured up to the  $(\frac{31}{2}^-)$  state in band G, the  $(\frac{37}{2}^-)$  state in band H, and the  $(\frac{25}{2}^-)$  state in band I. Effective lifetimes are given for the highest transition in each band for which a reliable line shape could be obtained from summing all possible clean gates generated by GFB. All gates used in the analysis of negative-parity states were projected from the triple-coincidence matrix which enhanced negative-parity transitions.

All mean lifetimes in band E were obtained by spectra GFB the transitions of interest. Most gates which showed coincidences with the 1035 keV transition in this band also showed coincidences with the 1030 keV transition in band G. Thus a simultaneous fit to both  $\gamma$ -ray line shapes was performed (see Fig. 4). The line shape of the 908 keV transition was corrupted at forward angles by an overlap with the 916 keV line in  $^{84}\text{Zr}$  [31] and the 915 keV line in  $^{86}\text{Zr}$  [32]. However, their effect at backward angles was greatly diminished, so reliable fits could be obtained at these angles.

The line shapes of the 1225, 1247, 1364, and 1532 keV transitions in band F were all obtained by summing spectra GFB these lines. For the 842, 969, and 1097 keV lines in this band, there were adequate statistics from adding spectra GFA these transitions to permit a GFA analysis. Band H has linking transitions of 1305 and 1425 keV to band F (see Fig. 1), and these relatively strong lines were used to measure the lifetimes of the 5742 keV  $(\frac{29}{2}^-)$  and 7088 keV  $(\frac{33}{2}^-)$  states, respectively. Unfortunately, the 1347 keV  $\gamma$  ray was too

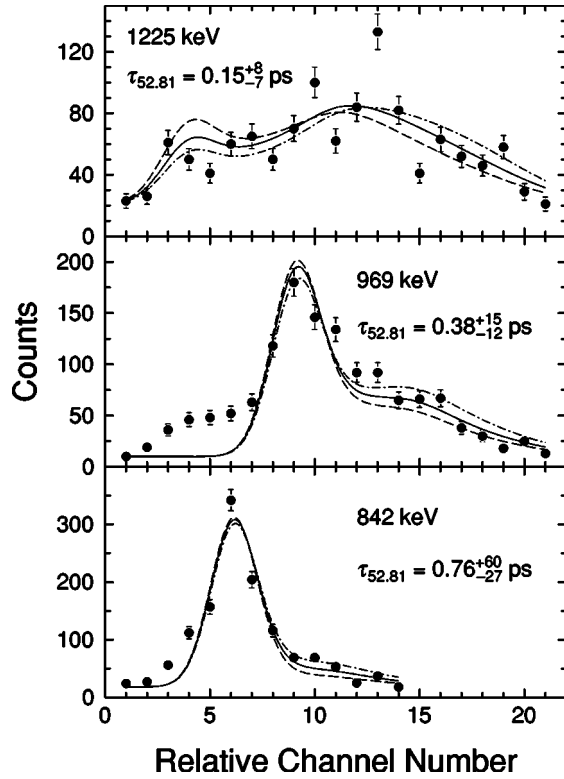


FIG. 7. Fits to the  $52.81^\circ$  line shapes of the 842, 969, and 1225 keV transitions in band F. The uncertainty limits of the best fit (solid curve) are indicated by the dashed and dash-dotted curves.

weak to perform an independent lifetime measurement of the 7088 keV ( $\frac{33}{2}^-$ ) state. Figure 7 illustrates the variation of line shapes, and hence the corresponding measured lifetimes, in band F.

Bands G and I were much more weakly populated than the yrast negative-parity bands E and F, but still allowed for a lifetime measurement of their most strongly populated states. In both bands, only a GFB analysis was possible due to limited statistics. In band G, both the 1174 and 1297 keV decays were used to measure the effective lifetime of the ( $\frac{31}{2}^-$ ) state. Mean lifetimes of the states below were then measured from the GFB line shapes of the 1030 and 822 keV transitions. As mentioned earlier, the 1030 keV line shape could only be resolved from that of the 1035 keV transition in band E through a simultaneous fit of both line shapes.

Statistics of the sum GFB spectra used for band I were very limited, especially for the 965 keV transition, where only a small number of gates could be used in order to eliminate the much stronger 969 keV line in band F. Still, only the  $34.95^\circ$  line shape could not be used to determine a lifetime for the ( $\frac{21}{2}^-$ ) parent state due to inadequate statistics. An analysis of the 811 keV transition in this band showed that three of four angles gave lifetimes well above 1 ps, so only a lower limit of 1 ps is given for the lifetime of the 2592-keV ( $\frac{17}{2}^-$ ) state.

### C. Transition strengths

Electric quadrupole transition strengths  $B(E2)$  were determined from the accepted lifetimes given in Table I, and

were used to calculate transition quadrupole moments  $|Q_i|$  from the rotational model according to

$$Q_i^2 = \frac{16\pi}{5} \langle IK20 | I-2K \rangle^{-2} B(E2, I \rightarrow I-2). \quad (1)$$

Both the  $B(E2)$  values and the  $Q_i$  moments are given in Table II. The branching ratios and the values of the  $K$  spin projection quantum number used for each band are also given in Table II.

Magnetic dipole transition strengths  $B(M1)$  were calculated using a quadrupole-dipole mixing ratio of  $\delta=0$  since  $B(M1)$  values are rather insensitive to  $\delta$  as long as it is small. Small values of  $\delta$  have been observed systematically for  $M1$  transitions in several neighboring nuclei ( $^{79}\text{Rb}$  [13], for example), and are thus expected for similar  $M1$  transitions in  $^{81}\text{Y}$ . All measurable magnetic dipole transition strengths are included in Table II.

## V. DISCUSSION

The most recent high-spin study of  $^{81}\text{Y}$  [22] revealed several sequences of states (many of which are shown in Fig. 1) which were interpreted as rotational bands within the context of the cranked-shell model. The kinematic moments of inertia  $J^{(1)}$  for the lowest positive-parity bands (bands A and B in Fig. 1) showed evidence for quasiparticle alignments near frequencies of  $\hbar\omega=0.67$  MeV (band A) and 0.74 MeV (bands A and B), followed by a convergence to the rigid rotor value ( $\approx 23 \hbar^2/\text{MeV}$  for  $\beta_2=0.2$ ) near a frequency of  $\hbar\omega=1.2$  MeV, as shown in Fig. 10 of Ref. [22]. The negative-parity bands in general showed a more gradual quasiparticle alignment followed by a trend toward the rigid rotor value, although these bands were not observed to as high a frequency as the positive-parity bands. An interesting feature of negative-parity band G (see Fig. 1) is the rather high, nearly constant moment of inertia of  $J^{(1)} \approx 26 \hbar^2/\text{MeV}$  [22], which is comparable to values typical for superdeformed bands in the mass  $A \approx 80$  region [33].

The lifetime measurements of this work were used to check the predictions of the cranked-shell model analysis as well as the predictions of Hartree-Fock-Bogolyubov (HFB) cranking calculations performed for the lowest positive- and negative-parity bands [18,22]. The results are discussed separately for the positive- and negative-parity bands below.

### A. Hartree-Fock-Bogolyubov cranking calculations

The evolution of shape and deformation with rotational frequency has previously been calculated [18,22] for the lowest positive- and negative-parity bands, and has been summarized in Fig. 8. Similar calculations have been performed in this work for other bands in order to illuminate the structural characteristics of the crossing bands and non-yrast states.

For this purpose, HFB cranking calculations [34] were performed which generate a total Routhian surface (TRS) plot in the  $(\beta_2, \gamma)$  plane at discrete rotational frequencies, using a Woods-Saxon potential and a short-range monopole pairing force. At each grid point, the Routhian was minimized with respect to the hexadecapole deformation  $\beta_4$ . The results of these calculations are discussed in Sec. V C 2.

TABLE II. Energies, spins, branching ratios  $R_B$ , electric quadrupole transition strengths  $B(E2)$ , magnetic dipole transition strengths  $B(M1)$ , and transition quadrupole moments  $|Q_t|$  in  $^{81}\text{Y}$ . Energies and spins were taken from Ref. [22]. Values of the  $K$  spin projection quantum number used for each band are included.

$E_x$ (keV)	$I_i^\pi$ ( $\hbar$ )	$E_\gamma$ (keV)	$R_B$ (%)	$B(E2)^a$ (W.u.)	$B(M1)$ $\mu_N^2$	$ Q_t $ (eb)	$E_x$ (keV)	$I_i^\pi$ ( $\hbar$ )	$E_\gamma$ (keV)	$R_B$ (%)	$B(E2)^a$ (W.u.)	$B(M1)$ $\mu_N^2$	$ Q_t $ (eb)
Band A													
			$K = \frac{5}{2}$				11518	$(\frac{45}{2}-)$	1712	100	$>17$		$>0.99$
13081	$(\frac{49}{2}+)$	1854	100	$>10$		$>0.77$	9805	$(\frac{41}{2}-)$	1532	100	$155^{+310}_{-113}$		$3.03^{+222}_{-145}$
11227	$(\frac{45}{2}+)$	1640	100	$47^{+284}_{-32}$		$1.68^{+277}_{-71}$	8274	$(\frac{37}{2}-)$	1364	100	$59^{+218}_{-36}$		$1.88^{+218}_{-69}$
9587	$(\frac{41}{2}+)$	1515	100	$123^{+369}_{-82}$		$2.73^{+273}_{-115}$	6909	$\frac{33}{2}-$	1247	70	$45^{+182}_{-23}$		$1.66^{+205}_{-49}$
8073	$\frac{37}{2}+$	1450	100	$56^{+67}_{-22}$		$1.85^{+89}_{-40}$			1167	30	$27^{+109}_{-14}$		$1.28^{+158}_{-38}$
6622	$\frac{33}{2}+$	1359	99	$70^{+23}_{-14}$		$2.09^{+32}_{-22}$	5662	$\frac{29}{2}-$	1225	100	$84^{+59}_{-27}$		$2.27^{+69}_{-40}$
5264	$\frac{29}{2}+$	1356	100	$95^{+76}_{-29}$		$2.46^{+84}_{-41}$	4437	$\frac{25}{2}-$	1097	100	$103^{+87}_{-43}$		$2.54^{+91}_{-60}$
3908	$\frac{25}{2}+$	1226	100	$64^{+24}_{-14}$		$2.06^{+36}_{-23}$	3340	$\frac{21}{2}-$	969	89	$107^{+44}_{-33}$		$2.63^{+49}_{-44}$
2682	$\frac{21}{2}+$	1033	100	$90^{+17}_{-14}$		$2.52^{+23}_{-21}$			482	11		$0.15^{+6}_{-5}$	
1650	$\frac{17}{2}+$	813	98	$110^{+38}_{-35}$		$2.93^{+46}_{-51}$	2371	$\frac{17}{2}-$	842	85	$102^{+58}_{-46}$		$2.63^{+67}_{-67}$
		171	2			$0.24^{+8}_{-8}$			421	11		$0.11^{+6}_{-5}$	
838	$\frac{13}{2}+$	569	87	$133^{+22}_{-16}$		$3.59^{+28}_{-23}$	Band G						
		156	13			$0.46^{+7}_{-6}$	$K = \frac{11}{2}$						
Band B													
			$K = \frac{5}{2}$				6385	$(\frac{31}{2}-)$	1297	40	$>8$		$>0.80$
5134	$(\frac{27}{2}+)$	1392	100	$>21$		$>1.16$			1174	60	$>20$		$>1.26$
3742	$(\frac{23}{2}+)$	1232	88	$53^{+41}_{-19}$		$1.89^{+63}_{-38}$	5211	$(\frac{27}{2}-)$	1030	100	$79^{+51}_{-22}$		$2.65^{+76}_{-41}$
		1060	12			$0.02^{+2}_{-1}$	4181	$(\frac{23}{2}-)$	1323	40	$4^{+11}_{-3}$		$0.66^{+64}_{-46}$
2510	$\frac{19}{2}+$	1030	76	$64^{+27}_{-19}$		$2.17^{+42}_{-35}$			822	49	$53^{+152}_{-48}$		$2.41^{+232}_{-166}$
		860	24			$0.05^{+2}_{-2}$	Band H						
1480	$\frac{15}{2}+$	798	59	$<71$		$<2.46$	$K = \frac{3}{2}$						
		642	41			$<0.09$	8517	$(\frac{37}{2}-)$	1430	100	$>20$		$>1.11$
Band E													
			$K = \frac{3}{2}$				7088	$(\frac{33}{2}-)$	1425	83	$79^{+198}_{-42}$		$2.19^{+190}_{-69}$
6468	$(\frac{31}{2}-)$	1380	100	$>16$		$>0.98$			1347	17	$22^{+54}_{-11}$		$1.14^{+99}_{-36}$
5089	$(\frac{27}{2}-)$	1196	100	$107^{+294}_{-54}$		$2.57^{+241}_{-75}$	5742	$(\frac{29}{2}-)$	1305	100	$40^{+54}_{-16}$		$1.56^{+84}_{-35}$
3893	$(\frac{23}{2}-)$	1035	100	$52^{+17}_{-13}$		$1.81^{+28}_{-24}$	Band I						
2858	$\frac{19}{2}-$	908	75	$74^{+51}_{-36}$		$2.22^{+66}_{-62}$	$K = \frac{1}{2}$						
		486	7			$0.05^{+4}_{-3}$	4713	$(\frac{25}{2}-)$	1157	100	$>16$		$>0.99$
Band F													
			$K = \frac{3}{2}$				3556	$(\frac{21}{2}-)$	965	100	$162^{+230}_{-82}$		$3.17^{+176}_{-95}$
							2592	$(\frac{17}{2}-)$	811	100	$<112$		$<2.66$

<sup>a</sup>1 W.u. =  $20.8 e^2 \text{fm}^4$ .

<sup>b</sup>Determined from the lifetime measured in Ref. [18].

Theoretical  $Q_t$  values were calculated for each band in which lifetimes were measured by using the  $\beta_2$  values obtained from the TRS plots. In order to make a proper comparison between experimental and theoretical values, the quadrupole deformation of the nuclear matter distribution derived from the TRS calculations was first related to the charge quadrupole deformation derived from the  $B(E2)$  strengths [35,36]. In order to take triaxiality into account, the high-spin limit for the  $\gamma$  dependence of  $Q_t$  [37,38] was used to determine the accepted theoretical  $Q_t$  values from those calculated assuming axial symmetry [35].

### B. Positive-parity bands

The transition quadrupole moments  $Q_t$  deduced from the measured lifetimes of yrast positive-parity states (bands A

and B in Fig. 1) are shown graphically in the middle panel of Fig. 9. In a rotational model picture, the yrast band shows a high degree of deformation (ranging from about  $\beta_2 = 0.20$  to  $0.40$ ). Both signature partners also show a rather gradual decrease in  $Q_t$  with increasing rotational frequency (or spin), although the favored signature values cover a wider frequency range. A possible disruption to this trend occurs in the favored band at a frequency of  $\hbar\omega = 0.75$  MeV, corresponding to the 1515 keV transition, but the rather large uncertainty associated with this value allows for the possibility of following the same pattern developed by the other values.

Calculations of the moments of inertia for the yrast positive-parity band [22] indicate that these changes in  $Q_t$  could be manifested by the onset of quasiparticle alignment, which first occurs for a pair of  $g_{9/2}$  neutrons [18] in the

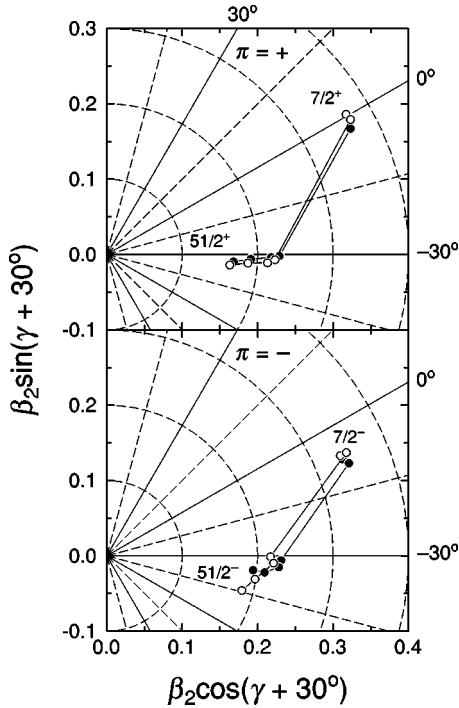


FIG. 8. Evolution of shape and deformation in the  $(\beta_2, \gamma)$  polar coordinate plane for a spin range of  $I = \frac{7}{2}$  to  $\frac{51}{2}$  in the yrast positive- (top) and negative- (bottom) parity bands of  $^{81}\text{Y}$ . Filled (open) circles represent the collective minima in the favored (unfavored) signature obtained from total Routhian surface calculations [18,22]. Each point represents an increase in rotational frequency of 0.1 MeV. Some values of the  $\gamma$ -deformation parameter are given surrounding the figure border.

favored (unfavored) band at  $\hbar\omega = 0.67$  MeV (0.74 MeV), followed by a  $g_{9/2}$  proton alignment [22] at  $\hbar\omega = 0.74$  MeV (0.81 MeV). However, the band crossings evident from changes in the moment of inertia are much more pronounced than the smooth variations observed for the  $Q_t$  values in the same frequency range. In general, the qualitative features of the moments of inertia are not reproduced in the  $Q_t$  moments. The moments of inertia do decrease in a frequency range ( $\hbar\omega \approx 1.0$  MeV) where the  $Q_t$  values are also decreasing, but here the moments of inertia appear to be converging toward the rigid rotor value.

Further evidence of band crossings as the cause for the reduction in the yrast band  $Q_t$  values comes from HFB cranking calculations (see Sec. V A and Refs. [18,22]). Theoretical  $Q_t$  values determined from these calculations are included in the middle panel of Fig. 9 and show good agreement with the experimental values. In this model, a change of shape occurs after the first quasiparticle alignment (predicted to occur at  $\hbar\omega \approx 0.5$  MeV) from nearly prolate ( $\gamma \approx 0^\circ$ ) to triaxial ( $\gamma \approx -30^\circ$ ), and is accompanied by an immediate reduction in deformation (from  $\beta_2 = 0.36$  to  $\beta_2 \approx 0.2$ ), which continues to decrease with increasing rotational frequency. This behavior is summarized graphically in the top panel of Fig. 8, which shows a polar plot of the values of the deformation parameters  $\beta_2$  and  $\gamma$  which correspond to total Routhian minima over a range of spins from

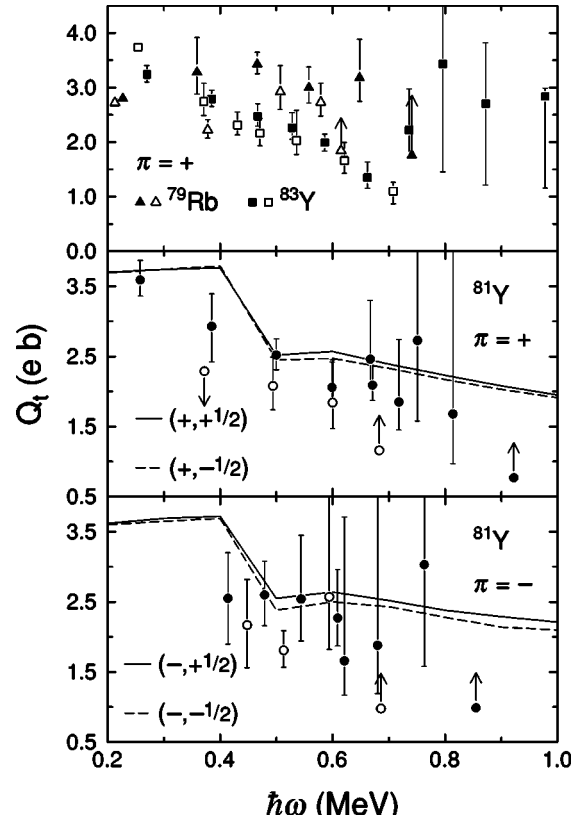


FIG. 9. Transition quadrupole moments  $Q_t$  as a function of rotational frequency for the positive-parity yrast bands of  $^{79}\text{Rb}$  [13] and  $^{83}\text{Y}$  [8,30] (top), yrast positive-parity bands A and B in  $^{81}\text{Y}$  (middle), and yrast negative-parity bands E and F in  $^{81}\text{Y}$  (bottom). Filled (open) symbols represent values obtained from signature  $\alpha = +\frac{1}{2}$  ( $\alpha = -\frac{1}{2}$ ) transitions. The solid and broken curves are theoretical predictions for the lowest positive- and negative-parity configurations from Hartree-Fock-Bogolyubov cranking calculations, and are labeled by their  $(\pi, \alpha)$  quantum numbers.

about  $\frac{7}{2}$  to  $\frac{51}{2}$ . Using the rotational model, the rather sharp drop in  $\beta_2$  corresponds to a similar drop in  $Q_t$ , which occurs more suddenly than those determined experimentally. It is possible that the dominant intrinsic quasiparticle configuration before the alignment (assigned to be the  $[422]_{5/2}^+$  Nilsson configuration [19,21]), which has a relatively larger deformation compared with that after the alignment, competes with the higher-seniority configuration after the band crossing and thus has the effect of “averaging” the  $Q_t$  moments of the two configurations, producing a more gradual change in  $Q_t$ .

An alternative interpretation of the observed reduction in the  $Q_t$  values with spin is that the amount of total spin available to the valence  $g_{9/2}$  quasiparticles becomes exhausted, and the yrast band thus gradually loses collectivity with increasing spin and eventually terminates. Evidence of this effect has already been demonstrated in the yrast band by comparing the excitation energies with a rigid rotor reference energy [22]. Near spin  $\frac{53}{2}^+$ , the energy difference between the two shows a characteristic parabola-like appearance, evidence for the high-energy cost of building the last spin states in this band. In such cases where termination occurs, the

corresponding HFB calculations usually show a tendency toward deformations approaching  $\beta_2 \approx 0$  with increasing spin. In contrast, HFB calculations for the yrast band in  $^{81}\text{Y}$  show Routhian minima near  $\beta_2 \approx 0.5$  at a frequency of 1.27 MeV [22].

A similar trend in the behavior of the  $Q_t$  moments with spin has been observed for the yrast positive-parity band in  $^{83}\text{Y}$  [8], as shown in the top panel of Fig. 9. The reduction in the  $Q_t$  values becomes more pronounced when compared to the behavior of those in  $^{79}\text{Rb}$  [13], which are included in the same figure. Due to the deformed shell gap at particle number 38, one might expect stronger evidence of termination (associated with falling  $Q_t$  values with spin) in  $^{79}\text{Rb}$ , rather than  $^{83}\text{Y}$ , but this is, in general, not the case. This suggests that band mixing effects may be playing a larger role in the fall of  $Q_t$  with spin in  $^{83}\text{Y}$  (and hence  $^{81}\text{Y}$ ) than band termination. However, it is difficult to draw firm conclusions because of the rather large uncertainties in the  $^{83}\text{Y}$   $Q_t$  values at high spin, and because the  $^{79}\text{Rb}$   $Q_t$  values were not measured to as high a spin as in  $^{83}\text{Y}$ .

The  $B(M1)$  strengths measured for the  $\Delta I=1$  transitions between bands A and B show the typical behavior observed in other odd- $A$  nuclei in this mass region. Relatively large (small)  $M1$  strength resides in transitions where the favored (unfavored) signature states decay to the unfavored (favored) signature states. An alternating pattern in the  $B(M1)$  values is obtained, along with a pronounced difference between the energies of adjacent states (signature splitting). These alternating  $B(M1)$  values are related to signature splitting [39–41] and can be understood in a picture where one quasiparticle moves in a rotating, deformed mean field [42]. A  $\Delta I=1$  decay from a favored signature state involves only a realignment of the single-particle spin without altering the core spin and hence generates strong  $M1$  radiation. The corresponding decay originating from an unfavored signature state requires a change in the core rotation which leads to reduced  $B(M1)$  strength.

### C. Negative-parity states

The  $Q_t$  values determined from the lifetimes of negative-parity states reveal the degree of collectivity of negative-parity structures in  $^{81}\text{Y}$ . In all, the collectivity of five bands was at least partially established.

#### 1. Bands F and E

The behavior of the  $Q_t$  values in the favored signature of the yrast negative-parity band (F in Fig. 1) is quite similar to the favored signature of the yrast positive-parity band (A in Fig. 1), as shown in the bottom panel of Fig. 9. The degree of collectivity is somewhat smaller near the band head (about 2.6 eb), which in a rotational model would correspond to  $\beta_2 \approx 0.3$ , and the reduction of  $Q_t$  with spin is somewhat smaller over a similar spin range. Still, the qualitative features are nearly the same as band A, despite the different quasiparticle configuration (suggested to be the  $\pi[301]_{\frac{3}{2}}^-$  configuration [22]). This difference, however, makes it very difficult to compare the yrast positive- and negative-parity

bands from a theoretical standpoint because of  $f-p$  orbital mixing in the negative-parity structures. The behavior of the  $Q_t$  values in the unfavored signature of the yrast negative-parity band (E in Fig. 1) is somewhat inconsistent over the spin range in which the measurement was made, so it is difficult to conclude if a similar decrease in  $Q_t$  with spin also exists in this sequence.

As in the case of the yrast positive-parity band, the likely cause of the gradual reduction in the  $Q_t$  values of band F appears to be from a band crossing following quasiparticle alignment. A cranked-shell model analysis of this band shows a smooth rise in the kinematic moments of inertia  $J^{(1)}$  at low frequencies, which has been interpreted [22] as a gradual alignment of a  $g_{9/2}$  proton pair. This smooth rise in  $J^{(1)}$  might explain the rather smooth decline in the  $Q_t$  values compared with that of band A, which in contrast had a much more pronounced change in  $J^{(1)}$  at the frequency of the first alignment. However, a sharp alignment occurs at a frequency of  $\hbar\omega = 0.62$  MeV (interpreted as a  $g_{9/2}$  neutron alignment [22]), and there does not appear to be any corresponding change in  $Q_t$  at this frequency. The conventional wisdom that higher moments of inertia correspond to larger collectivity does not seem strictly applicable in this case, as was the case in the positive-parity bands A and B.

Other evidence for band crossing effects influencing the amount of collectivity of band F comes from HFB calculations of this band [18]. The bottom panel of Fig. 8 summarizes the results of this calculation over the same spin range as similar calculations for band A (top panel of the figure). Although the reduction of  $\beta_2$  (and hence  $Q_t$ ) is predicted to occur quite suddenly near a frequency of  $\hbar\omega = 0.5$  MeV, the predicted frequency of the first band crossing, the quantitative values are quite similar to what was deduced experimentally. This is most easily observed in the comparison of the theoretical  $Q_t$  values (generated from the HFB calculations) with the experimental ones, shown in the bottom panel of Fig. 9 for both the favored and unfavored signatures. Good agreement is obtained between the theoretical and experimental values.

The  $B(M1)$  strengths of the  $\Delta I=1$  transitions between bands E and F are quite weak, as seen in Table II. Unlike the  $B(M1)$  values between bands A and B, there is very little if any evidence of an alternating pattern, and the reason awaits theoretical understanding. However, it is probably not surprising that there is very little signature splitting observed between bands E and F (see Fig. 1).

#### 2. Bands H, G, and I

Band F is crossed by band H near spin  $I = \frac{29}{2}$ . At this point, an interesting forking takes place in which both bands can be observed up to spin ( $\frac{53}{2}^-$ ). While the  $Q_t$  values in band F are falling with increasing spin in this region, they are still larger than the one intraband  $Q_t$  value of about 1.1 eb measured for band H (associated with the 1347 keV transition). Based on this value and that obtained for the 1305 keV interband transition to band F (1.6 eb), it appears that band H loses collectivity at the bottom of the sequence. The ( $\frac{33}{2}^-$ )  $\rightarrow$  ( $\frac{29}{2}^-$ ) 1425 keV crossover transition to band F

has a larger  $Q_t$  value than the  $^{33}_{2-} \rightarrow ^{29}_{2-}$  1247 keV intraband transition in band F, a good indicator that band F becomes more deformed and is more energetically favored than band H below spin  $^{33}_{2-}$ .

Band G was thought [22] to be a candidate for a superdeformed structure based on its consistently large moment of inertia of  $J^{(1)} \approx 26 \hbar^2/\text{MeV}$  over its observed spin range and its fragmentary decay near the band head at spin  $(^{19}_{2-})$ . However, while the deduced  $Q_t$  moments for this band imply strong deformations near  $\beta_2 = 0.3$ , these values are not considered to be superdeformed for this mass region ( $\beta_2 > 0.4$ ). By comparison, the largest deformations inferred for  $^{81}\text{Y}$  are near the bottom of the yrast positive-parity band where  $\beta_2$  approaches 0.4.

The structure of bands G and H were investigated with HFB calculations using an intrinsic quasiparticle configuration of  $\pi g_{9/2} \otimes \nu g_{9/2} \otimes \nu(fp)$ . The results of the calculation at three different rotational frequencies are shown in Fig. 10. The behavior of the TRS minima with frequency is reminiscent of that displayed by the yrast positive- and negative-parity states. Near-prolate minima ( $\gamma \approx 0^\circ$ ) at low frequency give way to triaxial shapes ( $\gamma \approx -30^\circ$ ) for frequencies greater than about 0.5 MeV. The degree of deformation appears to be both quantitatively and qualitatively similar to the yrast states as well.

The degree of collectivity in band I could only be roughly determined from the measurement of a single  $Q_t$  value associated with the 965 keV transition. The value of nearly 3.2 eb implies a large deformation of  $\beta_2 = 0.35$ , but must be viewed with caution in light of the rather large uncertainty associated with this value.

Non-yrast one-quasiparticle configurations having negative parity were also investigated with HFB calculations in order to compare with the experimental  $Q_t$  value determined for band I, which has been proposed to be based on the  $\pi[301]_{1/2}^-$  configuration [22]. These calculations revealed highly deformed ( $\beta_2 \approx 0.35$ ), near prolate shapes for frequencies below about 0.5 MeV, where once again the favored shape becomes triaxial with a deformation that decreases with spin. The deformation predictions at low frequency appear to be in good agreement with the result inferred from the measured lifetime of the  $(^{21}_{2-})$  state.

## VI. SUMMARY

Lifetimes of 34 high-spin states in  $^{81}\text{Y}$  were measured using the Doppler-shift attenuation method at four average detector angles. The  $^{58}\text{Ni}(^{32}\text{S}, 2ap)$  reaction at 135 MeV was used to populate the excited states, and a thick Ta backing material intimately attached to the target allowed for line-shape analysis. The GAMMASPHERE array and the MICROBALL were used to detect multi- $\gamma$  coincidences with evaporated charged particles. Clean line shapes from this weak reaction product were obtained through triple- $\gamma$  coincidences along with gating on the  $2ap$  reaction channel. Lifetimes were measured whenever possible by fitting line shapes obtained from gating above the transition of interest. In these cases, side-feeding times could be measured by comparing line

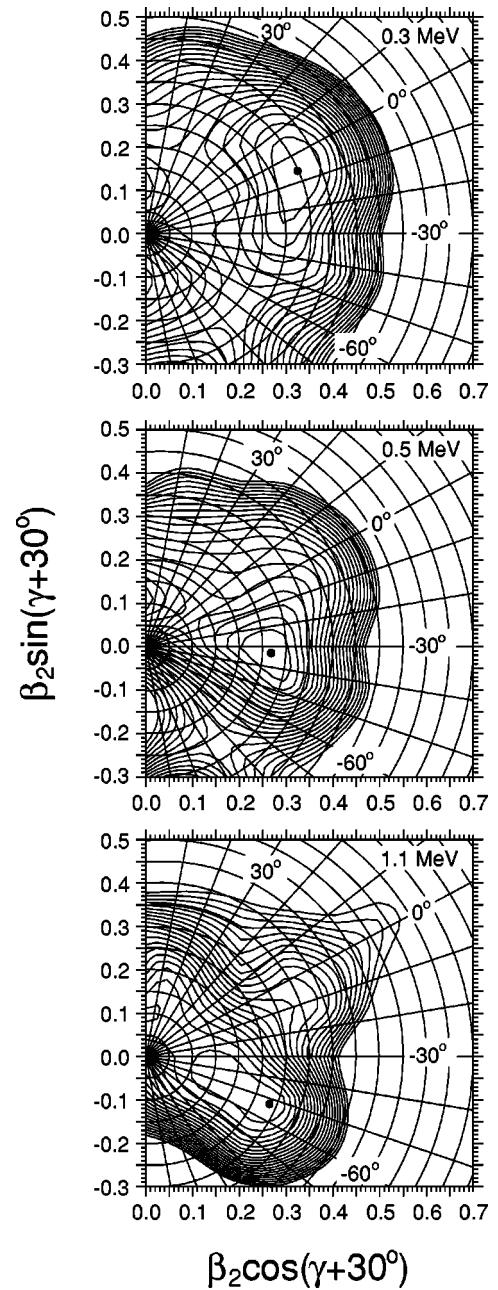


FIG. 10. Total Routhian surface calculations for the  $\pi g_{9/2} \otimes \nu g_{9/2} \otimes \nu(fp)$  intrinsic configuration in  $^{81}\text{Y}$  at three different rotational frequencies. The spacing between contour lines is 200 keV.

shapes fitted from spectra gated from above and below. The measured side-feeding times were then used to help determine the feeding corrections for states where the decay line shape could only be obtained reliably by gating from below.

Transition quadrupole moments  $Q_t$  calculated from the lifetimes in the yrast positive-parity bands A and B show a gradual decrease from 3.6 eb at low spin to 1.7 eb at spin  $(^{45}_{2+})$ . These results are in good agreement with the predictions of HFB cranking calculations, which also show decreasing  $Q_t$  values with spin, although the decrease happens more suddenly due to the onset of a shape change from nearly prolate to triaxial. A cranked-shell model analysis

shows that this is likely caused by an alignment of a  $g_{9/2}$  neutron pair, followed by an alignment of a  $g_{9/2}$  proton pair.

The falling  $Q_1$  values with spin in the favored yrast negative-parity band F closely resemble those of band A, except the decrease is even more gradual. HFB and cranked-shell model calculations together suggest that this decrease is due to the alignment of a  $g_{9/2}$  proton pair, followed by an alignment of a  $g_{9/2}$  neutron pair at even higher spin. Bands G and H, which cross bands E and F respectively at high spin, show a tendency for an increase in the amount of collectivity with increasing spin near the crossing frequency. However, HFB calculations predict that these structures should also show a decrease in collectivity with spin, although not enough lifetimes could be measured to provide experimental verification. Band I also shows large deformation at low spins, in agreement with HFB calculations.

## ACKNOWLEDGMENTS

This work was supported in part by the Purdue Research Foundation (PUC), the National Science Foundation under Grant No. PHY-9523974 (FSU), and the Department of Energy under Contract Nos. DE-AC05-76OR00033 (UNISOR), DE-AC05-96OR22464 (ORNL), DE-FG05-88ER40406 (WU), and DE-AC03-76SF00098 (LBNL). We thank W. Nazarewicz for providing the results of his Hartree-Fock-Bogolyubov cranking calculations, and the staff of the LBNL 88-in. Cyclotron facility for providing excellent research conditions. F.C. acknowledges support from Colciencias (Bogotá), Contract No. 222-96. R.A.K. would like to thank S. Haring for invaluable support and A. Afanasjev for informative discussions during the writing of this manuscript.

- 
- [1] R. Diller, K.P. Lieb, L. Lühmann, T. Osipowicz, P. Sona, B. Wörmann, L. Cleemann, and J. Eberth, *Z. Phys. A* **321**, 659 (1985).
- [2] E.K. Warburton, J.W. Olness, C.J. Lister, J.A. Becker, and S.D. Bloom, *J. Phys. G* **12**, 1017 (1986).
- [3] L. Funke, G. Winter, J. Döring, L. Käubler, H. Prade, R. Schwengner, E. Will, Ch. Protopostov, W. Andrejtscheff, L.G. Kostova, P.O. Lipas, and R. Wirowski, *Nucl. Phys.* **A541**, 241 (1992).
- [4] J. Reif, G. Winter, R. Schwengner, H. Prade, and L. Käubler, *Nucl. Phys.* **A587**, 449 (1995).
- [5] R. Schwengner, J. Reif, H. Schnare, G. Winter, T. Servene, L. Käubler, H. Prade, M. Wilhelm, A. Fitzler, S. Kasemann, E. Radermacher, and P. von Brentano, *Phys. Rev. C* **57**, 2892 (1998).
- [6] P.C. Womble, J. Döring, T. Glasmacher, J.W. Holcomb, G.D. Johns, T.D. Johnson, T.J. Petters, M.A. Riley, V.A. Wood, S.L. Tabor, and P. Semmes, *Phys. Rev. C* **47**, 2546 (1993).
- [7] G.D. Johns, K.A. Christian, R.A. Kaye, S.L. Tabor, G. García-Bermúdez, M.A. Cardona, A. Filevich, H. Somacal, and L. Szybisz, *Phys. Rev. C* **53**, 1541 (1996).
- [8] T.D. Johnson, A. Aprahamian, C.J. Lister, D.J. Blumenthal, B. Crowell, P. Chowdhury, P. Fallon, and A.O. Macchiavelli, *Phys. Rev. C* **55**, 1108 (1997).
- [9] A.V. Afanasjev and I. Ragnarsson, *Nucl. Phys.* **A591**, 387 (1995).
- [10] C.J. Gross, J. Heese, K.P. Lieb, S. Ulbig, W. Nazarewicz, C.J. Lister, B.J. Varley, J. Billowes, A.A. Chishti, J.H. McNeill, and W. Gelletly, *Nucl. Phys.* **A501**, 367 (1989).
- [11] M.A. Cardona, G. García Bermúdez, A. Filevich, and E. Achterberg, *Phys. Rev. C* **42**, 591 (1990).
- [12] T.D. Johnson, J.W. Holcomb, P.C. Womble, P.D. Cottle, S.L. Tabor, F.E. Durham, S.G. Buccino, and M. Matsuzaki, *Phys. Rev. C* **42**, 2418 (1990).
- [13] J.W. Holcomb, J. Döring, T. Glasmacher, G.D. Johns, T.D. Johnson, M.A. Riley, P.C. Womble, and S.L. Tabor, *Phys. Rev. C* **48**, 1020 (1993).
- [14] A. Harder, A. Jungclaus, M.K. Kabadiyski, D. Kast, K.P. Lieb, D. Rudolph, M. Weiszflog, T.D. Johnson, G. Winter, C.J. Gross, R.A. Cunningham, W. Gelletly, J. Simpson, D.D. Warner, I.G. Bearden, T. Shizuma, G. Sletten, D. Foltescu, H.A. Roth, Ö. Skeppstedt, and B.J. Varley, *Phys. Rev. C* **55**, 1680 (1997).
- [15] R.A. Kaye, J. Döring, J.W. Holcomb, G.D. Johns, T.D. Johnson, M.A. Riley, G.N. Sylvan, P.C. Womble, V.A. Wood, S.L. Tabor, and J.X. Saladin, *Phys. Rev. C* **54**, 1038 (1996).
- [16] D.F. Winchell, V.Q. Wood, J.X. Saladin, I. Birriel, C. Baktash, M.J. Brinkman, H.-Q. Jin, D. Rudolph, C.-H. Yu, M. Devlin, D.R. LaFosse, F. Lerma, D.G. Sarantites, G. Sylvan, S. Tabor, R.M. Clark, P. Fallon, I.Y. Lee, and A.O. Macchiavelli, *Phys. Rev. C* **61**, 044322 (2000).
- [17] J. Heese, K.P. Lieb, S. Ulbig, B. Wörmann, J. Billowes, A.A. Chishti, W. Gelletly, C.J. Lister, and B.J. Varley, *Phys. Rev. C* **41**, 603 (1990).
- [18] T.D. Johnson, A. Raguse, C.J. Gross, M.K. Kabadiyski, K.P. Lieb, D. Rudolph, M. Weiszflog, T. Burkardt, J. Eberth, and S. Skoda, *Z. Phys. A* **350**, 189 (1994).
- [19] C.J. Lister, R. Moscrop, B.J. Varley, H.G. Price, E.K. Warburton, J.W. Olness, and J.A. Becker, *J. Phys. G* **11**, 969 (1985).
- [20] A. Raguse, C.J. Gross, M.K. Kabadiyski, K.P. Lieb, D. Rudolph, M. Weiszflog, T. Burkardt, S. Skoda, Ö. Skeppstedt, M.A. Bentley, W. Gelletly, H.G. Price, J. Simpson, J.L. Durell, and B.J. Varley, in *Proceedings of the 8th International Symposium on Capture Gamma-Ray Spectroscopy and Related Topics, Fribourg 1993* (World Scientific, Singapore, 1994), p. 444.
- [21] S. Mitarai, T. Kuroyanagi, A. Odahara, J. Mukai, H. Tomura, S. Suematsu, T. Morikawa, D. Jerrestam, J. Nyberg, G. Sletten, A. Atac, M. Piiparinen, S.E. Arnell, D. Foltescu, H.A. Roth, and Ö. Skeppstedt, *Nucl. Phys.* **A557**, 381c (1993).
- [22] H. Schnare, G. Winter, L. Käubler, J. Reif, R. Schwengner, J. Döring, G.D. Johns, S.L. Tabor, C.J. Gross, Y.A. Akovali, C. Baktash, D.W. Stracener, F.E. Durham, P.F. Hua, M. Korolija, D.R. LaFosse, D.G. Sarantites, I.Y. Lee, A.O. Macchiavelli, W. Rathbun, and A. Vander Molen, *Phys. Rev. C* **56**, 729 (1997).
- [23] D.R. LaFosse, P.-F. Hua, D.G. Sarantites, C. Baktash, Y.A. Akovali, M. Brinkman, B. Cederwall, F. Cristancho, J. Döring, C.J. Gross, H.-Q. Jin, M. Korolija, E. Landulfo, I.Y. Lee, A.O. Macchiavelli, M.R. Maier, W. Rathbun, J.X. Saladin, D.W.

- Stracener, S.L. Tabor, A. Vander Mollen, and T.R. Werner, Phys. Lett. B **354**, 34 (1995).
- [24] I.Y. Lee, Nucl. Phys. **A520**, 641c (1990).
- [25] D.G. Sarantites, P.-F. Hua, M. Devlin, L.G. Sobotka, J. Elson, J.T. Hood, D.R. LaFosse, J.E. Sarantites, and M.R. Maier, Nucl. Instrum. Methods Phys. Res. A **381**, 418 (1996).
- [26] M. Wiedeking, R.A. Kaye, G.Z. Solomon, S.L. Tabor, J. Döring, G.D. Johns, F. Cristancho, M. Devlin, F. Lerma, D.G. Sarantites, I.Y. Lee, and A.O. Macchiavelli, Phys. Rev. C **62**, 024316 (2000).
- [27] E.F. Moore, P.D. Cottle, C.J. Gross, D.M. Headly, U.J. Hüttmeier, S.L. Tabor, and W. Nazarewicz, Phys. Rev. C **38**, 696 (1988).
- [28] J.F. Ziegler, J.P. Biersack, and U. Littmark, *The Stopping and Range of Ions in Matter* (Pergamon, New York, 1985).
- [29] <http://www.SRIM.org>
- [30] F. Cristancho, K.P. Lieb, J. Heese, C.J. Gross, W. Fieber, Th. Osipowicz, S. Ulbig, K. Bharuth-Ram, S. Skoda, J. Eberth, A. Dewald, and P. von Brentano, Nucl. Phys. **A501**, 118 (1989).
- [31] S. Chattopadhyay, H.C. Jain, and J.A. Sheikh, Phys. Rev. C **53**, 1001 (1996).
- [32] J. Döring, Y.A. Akovali, C. Baktash, F.E. Durham, C.J. Gross, P.F. Hua, G.D. Johns, M. Korolija, D.R. LaFosse, I.Y. Lee, A.O. Macchiavelli, W. Rathbun, D.G. Sarantites, D.W. Stracener, G.Z. Solomon, S.L. Tabor, A. Vander Molen, A.V. Afanasjev, and I. Ragnarsson, Phys. Rev. C **61**, 034310 (2000).
- [33] F. Lerma, M. Devlin, D.R. LaFosse, D.G. Sarantites, R. Wyss, C. Baktash, R.M. Clark, I.Y. Lee, A.O. Macchiavelli, R.W. MacLeod, D. Soltysik, and S.L. Tabor, Phys. Rev. Lett. **83**, 5447 (1999).
- [34] W. Nazarewicz, J. Dudek, R. Bengtsson, T. Bengtsson, and I. Ragnarsson, Nucl. Phys. **A435**, 397 (1985).
- [35] W. Nazarewicz, M.A. Riley, and J.D. Garrett, Nucl. Phys. **A512**, 61 (1990).
- [36] J. Dudek, W. Nazarewicz, and P. Olanders, Nucl. Phys. **A420**, 285 (1984).
- [37] I. Hamamoto and B.R. Mottelson, Phys. Lett. **132B**, 7 (1983).
- [38] P. Ring, A. Hayashi, K. Hara, H. Emling, and E. Grosse, Phys. Lett. B **110B**, 423 (1982).
- [39] I. Hamamoto and H. Sagawa, Nucl. Phys. **A327**, 99 (1979).
- [40] I. Hamamoto, Phys. Lett. **106B**, 281 (1981).
- [41] F. Dönau, Nucl. Phys. **A471**, 469 (1987).
- [42] M. Matsuzaki, Phys. Rev. C **39**, 691 (1989).